Detection of Majorana Kramers Pairs Using a Quantum Point Contact

Jian Li, Wei Pan, B. Andrei Bernevig, and Roman M. Lutchyn

Phys. Rev. Lett. **117**, 046804 — Published 20 July 2016

DOI: 10.1103/PhysRevLett.117.046804

Detection of Majorana Kramers pairs using a quantum point contact

Jian Li,[1] Wei Pan,[2] B. Andrei Bernevig,[1] and Roman M. Lutchyn[3]

[1] *Department of Physics, Princeton University, Princeton, NJ 08544, USA*
[2] *Sandia National Laboratories, Albuquerque, NM 87185, USA*
[3] *Station Q, Microsoft Research, Santa Barbara, California 93106-6105, USA*

(Dated: July 7, 2016)

We propose a setup that integrates a quantum point contact (QPC) and a Josephson junction on a quantum spin Hall sample, experimentally realizable in InAs/GaSb quantum wells. The confinement due to both the QPC and the superconductor results in a Kramers pair of Majorana zero-energy bound states when the superconducting phases in the two arms differ by an odd multiple of π across the Josephson junction. We investigate the detection of these Majorana pairs with the integrated QPC, and find a robust switching from normal to Andreev scattering across the edges due to the presence of Majorana Kramers pairs. Such a switching of the current represents a qualitative signature where multi-terminal differential conductances oscillate with alternating signs when the external magnetic field is tuned. We show that this qualitative signature is also present in current cross-correlations. Thus, the change of the backscattering current nature affects both conductance and shot noise, the measurement of which offers a significant advantage over quantitative signatures such as conductance quantization in realistic measurements.

In the pursuit of Majorana zero-energy modes [1–6] in topological superconductors several experimental and theoretical directions are being explored. Most noticeably, these include topological insulator/superconductor structures [7–11], semiconductor-superconductor heterostructures [12–23], and magnetically-ordered metallic systems coupled to an s-wave superconductor [24–32]. In all cases, proximity to superconductivity (SC) leads to the formation of the Majorana zero-energy bound states localized at the defects such as vortices and domain walls. Such defects have been predicted to obey non-Abelian braiding statistics [33–35], and, as such, might be useful for topological quantum computation [36–38]. The detection of MBSs often involves measurements of transport signatures such as zero-bias anomalies [16, 18, 39–41], quantized conductance [39, 42, 43], or fractional Josephson effect [8, 13, 36, 44, 45]. Most of these signatures, however, can be obscured by real-world problems like disorder [46–48] and quasi-particle poisoning [49, 50], making the detection of MBSs challenging.

In this paper, we propose a setup for preparing and observing MBSs in systems exhibiting quantum spin Hall (QSH) effect [51–53], such as HgTe quantum wells [52–54], and InAs/GaSb quantum wells [10, 11, 55–57]. The setup, illustrated in Fig. 1, has a built-in quantum point contact (QPC) with a conventional superconductor (SC) junction covering a half of the constriction. The two parts of the SC are connected far away from the QPC region, and consequently the SC phase difference φ across the SC junction can be tuned by a weak perpendicular magnetic field. A pair of zero-energy MBSs is localized at the junction when φ is an odd multiple of π [8, 58]. At these points, time-reversal symmetry (TRS) applies approximately as long as the magnetic field that creates the phase difference for the SC arms is weak enough, and the MBSs form a Kramers pair. Using the scattering approach for noninteracting electrons [59, 60], we analyze the transport signatures related to these MBSs and propose several ways to measure them using the QPC. The advantages of this proposal are twofold: first, several key steps such as the experimental realization of a QPC, as well as proximity induced pairing in the edge states, in an InAs/GaSb QSH sample have been already performed [61]; second, our proposed signature is qualitative, and does not rely on quantization of differential conductances that is difficult to realize due to thermal broadening.

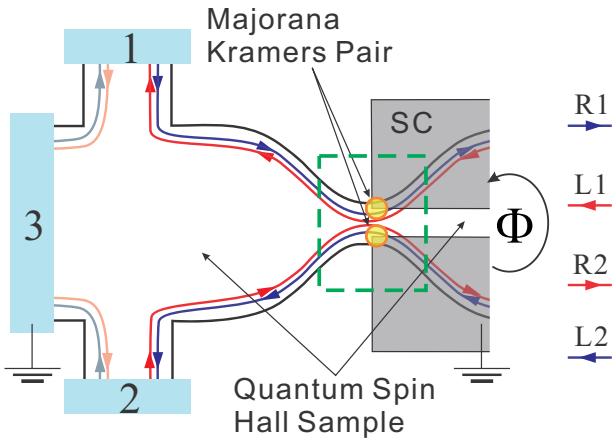

FIG. 1. Our proposed setup: a quantum point contact build in a quantum spin Hall sample is half covered by a Josephson junction; three metallic contacts of a (half) Hall-bar configuration are away from the point contact, with contact 3 always grounded.

We start by analytically finding the bound-state solutions at the interface between the quantum point contact and the SC (see Fig. 1 highlighted region). In the inter-

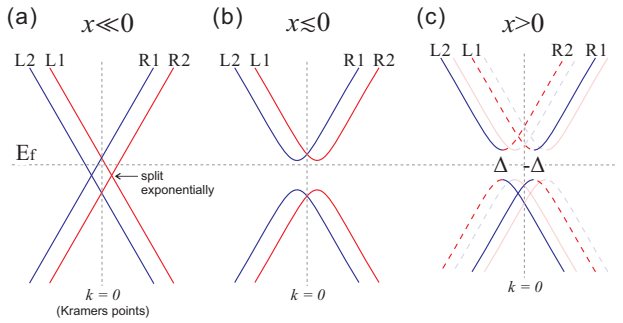

FIG. 2. Schematic explanation of the origin of the Majorana Kramers pairs.

face region, the effective Hamiltonian is given by

$$\begin{aligned} H = \int dx \sum_{n=1,2} \Big[\psi^\dagger_{Rn}(\hbar v_F \hat{k} - \mu)\psi_{Rn} + \psi^\dagger_{Ln}(-\hbar v_F \hat{k} - \mu)\psi_{Ln}\Big] \\ + \sum_{n=1,2} \Delta_n(x) e^{i\varphi_n(x)} \psi^\dagger_{Rn}\psi^\dagger_{Ln} + h.c. \\ + m(x)(\psi^\dagger_{R1}\psi_{L2} + \psi^\dagger_{L1}\psi_{R2}) + h.c. \\ + f(x)(\psi^\dagger_{R1}\psi_{R2} - \psi^\dagger_{L1}\psi_{L2}) + h.c., \end{aligned} \tag{1}$$

where $\psi_{R/Ln} \equiv \psi_{R/Ln}(x)$ is the fermionic field (annihilation) operator near the Fermi energy for the right/left moving edge states along the upper ($n = 1$) or lower ($n = 2$) edge, v_F is the Fermi velocity, $\hat{k} \equiv -i\partial_x$, and all $\Delta_n(x)$, $m(x)$ and $f(x)$ are real without loss of generality. Physically, m and f represent the hybridization gaps possible when the two edges of the QSH sample approach near the QPC; Δ is the induced SC gap with phases φ_1 and φ_2 in different arms (see Fig. 1). This Hamiltonian transforms under time-reversal and particle-hole symmetries (PHS) as follows:

$$TH(\varphi_1, \varphi_2)T^{-1} = H(-\varphi_1, -\varphi_2), \tag{2}$$

$$PH(\varphi_1, \varphi_2)P^{-1} = -H(\varphi_1, \varphi_2). \tag{3}$$

Here, by definition, $T\psi_{Rn}T^{-1} = s_n\psi_{Ln}$, $T\psi_{Ln}T^{-1} = -s_n\psi_{Rn}$ with s_1=1 and s_2=−1, $P\psi_{R/Ln}P^{-1} = \psi^\dagger_{R/Ln}$, $TaT^{-1} = a^*$ and $PaP^{-1} = a^*$ if a is a number. For simplicity, we further assume $\Delta_n(x) = s_n\theta(x)\Delta$, $m(x) = \theta(-x)m$, $f(x) = \theta(-x)f$ with $\theta(x)$ the Heaviside step function and $\Delta, m, f > 0$, as well as

$$\varphi_1(x) = (1 - \epsilon_0 x)\varphi, \quad \varphi_2(x) = (\epsilon_0 x)\varphi \quad (\epsilon_0 \geq 0). \tag{4}$$

Physically, ϵ_0 is roughly proportional to the inverse of the circumference of the SC that encloses the magnetic flux. We assume ϵ_0 to be sufficiently small such that both φ_1 and φ_2 are slowly varying at the length scale of the SC coherence length $\xi = \hbar v_F/\Delta$. If $\epsilon_0 \neq 0$, there is a finite TRS-breaking splitting energy between two MBSs $\delta E = \hbar v_F \epsilon_0 \varphi/2$ even if φ is an integer multiple of π [cf. Eq. (2)].

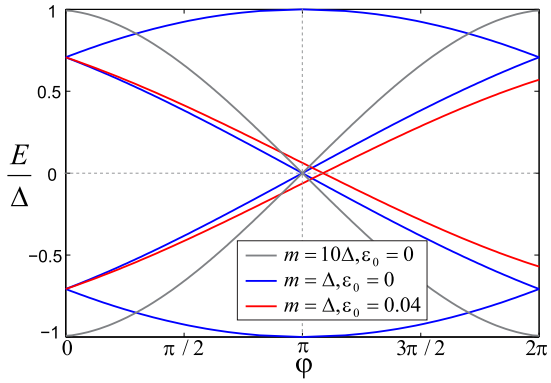

FIG. 3. Spectra of the subgap states obtained numerically from Eq. (5). Cases are compared between strong (grey line) and mild (blue line) point contact constriction, as well as between constant (blue line) and spatially varying (red line) pairing phases. In all cases we assume $\mu = 0$.

The existence of a Kramers pair of MBSs in the limit of $\epsilon_0 = 0$ is based on a simple physical argument. In Fig. 2a we present the system's every dispersion in the normal region far from the QPC ($x \ll 0$), featured by the two gapless one-dimensional Dirac dispersions of the lower and upper QSH edges. As the edges get closed together near the QPC ($x \lesssim 0$), they hybridize and open a trivial gap at non-Kramers points (Fig. 2b). On the SC side ($x > 0$), a SC gap (larger than the hybridization gap, which is always the case when $x \gg 0$) is present at the Fermi level (which can be tuned by a gate) to create another insulator. This is a gapped superconductor, but, it is a topological one (Fig. 2c). Notice that R_1, R_2 are right movers giving two $k > 0$ Fermi points on the upper and lower edges, as such, the superconducting gaps differ by a sign on the two $k > 0$ Fermi points when there is a π phase shift in the two arms of the superconductor. Thus, at $x > 0$ we have a time-reversal topological superconductor. A Kramers pair of MBS appears when the topological superconductor is put next to a trivial insulator $x \lesssim 0$. These qualitative arguments agree well with the analytic solution discussed below.

In the subgap regime, namely $|E| < \min(m - |\mu|, \Delta - |\delta E|)$, the solutions of bound states can be obtained by matching eigenstate wavefunctions at the interface (see Supplemental Material[62] Sec. I.C). The eigenvalues are determined by the following equation

$$[e^{i(\alpha-\beta-2\gamma_-)} - e^{i\varphi}][e^{i(\beta-\alpha-2\gamma_+)} - e^{i\varphi}] = 0, \tag{5}$$

where $\cos\alpha = (\mu + E)/m$, $\cos\beta = (\mu - E)/m$, $\cos\gamma_\pm = (\delta E \pm E)/\Delta$ with $\alpha, \beta, \gamma_\pm \in (0, \pi)$. Eq. (5) is particle-hole symmetric, as changing the sign of E exchanges the two terms on its left-hand side. In the limit of pinched-off QPC ($m \to \infty$), we obtain $E = \pm(\Delta\cos\varphi/2 \pm \delta E)$ [8, 44]. The full subgap spectra in generic cases can be solved numerically, as exemplified in Fig. 3.

Zero-energy solutions should satisfy $\alpha = \beta$ and $\gamma_+ =$

$\gamma_- = \gamma = \arccos(\delta E/\Delta) \in (0,\pi)$, hence Eq. (5) is reduced to

$$e^{i(\varphi+2\gamma)} = 1. \tag{6}$$

When $\epsilon_0 = 0$, the zero energy solutions, occurring iff $\varphi = (2l+1)\pi$ with l being an integer, define two Majorana operators

$$\chi_1 = \int dx\big[(\tilde{\psi}^{(-)}_{R1} + i\tilde{\psi}^{(+)}_{L1} + i\tilde{\psi}^{(+)}_{R2} + \tilde{\psi}^{(-)}_{L2}) + h.c.\big], \tag{7}$$

$$\chi_2 = \int dx\big[(i\tilde{\psi}^{(+)}_{R1} + \tilde{\psi}^{(-)}_{L1} + \tilde{\psi}^{(-)}_{R2} + i\tilde{\psi}^{(+)}_{L2}) + h.c.\big], \tag{8}$$

where $\tilde{\psi}^{(\pm)}_{R/Ln} = [\theta(-x)e^{(m\sin\alpha)x}(\cos fx \pm \sin fx) + \theta(x)e^{-\Delta x}e^{s_{R/L}i\mu x}]\psi_{R/Ln}$ with $s_{R/L} = \mp 1$ (here we set $\hbar v_F = 1$). As a result of TRS in this idealized case, χ_1 and χ_2 form a Kramers pair: $T\chi_1 T^{-1} = \chi_2$ and $T\chi_2 T^{-1} = -\chi_1$ [63]. When ϵ_0 is finite but small (i.e. $|\delta E|/\Delta \ll 1$), Eq. (6) yields $\varphi = (2l+1)\pi/(1-\epsilon_0\xi)$. The zero-energy solutions shift to φ's different from $(2l+1)\pi$, owing to the finite penetration of the bound states into the gapped SC, and are no longer exact Kramers partners (see Supplemental Material[62] Sec. I.D). We will neglect this subtlety in the following by assuming ϵ_0 to be sufficiently small.

Having established the presence of the MBSs at the QPC-SC interface, we now discuss their detection. To this end, the incorporation of the QPC in our proposed setup was particularly useful as the QSH edge states reflected at the QPC naturally become probes of the MBSs. In this case, the low-energy ($E < \Delta$) effective Hamiltonian in the presence of a Majorana Kramers pair, constrained by TRS, has a generic form

$$H_\pi = -i\int_{-\infty}^{+\infty} d\tilde{x}\,\Big\{\psi^\dagger_+\partial_{\tilde{x}}\psi_+ - \psi^\dagger_-\partial_{\tilde{x}}\psi_- + \delta(\tilde{x})\big[\chi_1(t_+\psi_+ + t_-\psi_- + h.c.) + \chi_2(t^*_-\psi_+ - t^*_+\psi_- + h.c.)\big]\Big\}, \tag{9}$$

where $\tilde{x}$ stands for the unfolded coordinate such that $\psi_+(\tilde{x}) \equiv \theta(-\tilde{x})\psi_{R1}(\tilde{x}) + \theta(\tilde{x})\psi_{L2}(-\tilde{x})$ and $\psi_-(\tilde{x}) \equiv \theta(-\tilde{x})\psi_{R2}(\tilde{x}) + \theta(\tilde{x})\psi_{L1}(-\tilde{x})$; $t_\pm$ stands for the coupling between the MBSs and $\psi_\pm$. H_π is manifestly time-reversal symmetric. The scattering matrix that relates the current amplitudes of the outgoing (electron and hole) components of $\psi_\pm$ to those of the incoming components can be obtained by using the formula [9]

$$S_\pi(E) = \mathbb{1} - iW^\dagger(E + \frac{i}{2}WW^\dagger)^{-1}W, \tag{10}$$

$$W = -i\begin{pmatrix} t_+ & t_- & t^*_+ & t^*_- \\ t^*_- & -t^*_+ & t_- & -t_+ \end{pmatrix}, \tag{11}$$

where W is the coupling matrix between the scattering modes and the Majorana pair. This yields

$$S_\pi(E) = \frac{1}{iE-\Gamma}\begin{pmatrix} 0 & iE & -A & C \\ iE & 0 & C^* & -A \\ A & C^* & 0 & iE \\ C & A & iE & 0 \end{pmatrix}, \tag{12}$$

where $\Gamma = |t_+|^2 + |t_-|^2$, $A = t_+t_- - (t_+t_-)^*$, $C = t_+^2 + (t_-^2)^*$. We have chosen the outgoing basis in Eq. (12) so that both the incoming and the outgoing bases are ordered as (1e, 2e, 1h, 2h), where 1(2) stands for the upper(lower) arm and e(h) stands for the electron(hole) component of the original edge channels (cf. Fig. 1). We immediately see that at $E = 0$, all normal scattering processes, corresponding to the diagonal blocks in Eq. (12), vanish; only local (A) and crossed (C) Andreev scatterings remain. This scenario represents a fixed point for the scattering corresponding to the presence of a Majorana Kramers pair.

Away from this fixed point, the consequence of lifted degeneracy at zero-energy can be investigated perturbatively by including an additional term $H_M(\varphi) = iE_\varphi\chi_1\chi_2$ ($E_\pi = 0$) into Hamiltonian (9). In terms of the scattering matrix, this amounts to replacing E on the right-hand side of Eq. (10) by $E + E_\varphi\sigma_y$ with σ_y the Pauli matrix. To the lowest order in E_φ, the correction to the scattering matrix in Eq. (12) is given by

$$\delta S(E) = \frac{E_\varphi}{(iE-\Gamma)^2}\begin{pmatrix} -C & -A & -\Gamma & 0 \\ A & C^* & 0 & \Gamma \\ -\Gamma & 0 & -C^* & A \\ 0 & \Gamma & -A & C \end{pmatrix}, \tag{13}$$

which suggests a suppression of crossed Andreev reflection and simultaneously an enhancement of normal scattering processes when E_φ becomes large compared to $\max(|E|,\Gamma)$. Indeed this situation corresponds to another (trivial) fixed point as shown next through symmetry analysis.

In order to understand the scattering of helical edge states at the QPC-SC interface in a more general setting, we go back to the original Hamiltonian (1) and define the scattering matrix generically as [64]

$$S_{n'\nu',n\nu}(E) = i\hbar v_F G^R_{n'\nu',n\nu}(x'_0, x_0; E), \tag{14}$$

where $n, n' = 1, 2$ stand for the lateral edges, $\nu, \nu' = e, h$ stand for electron or hole channels, and the retarded Green's functions $G^R_{n'\nu',n\nu}(x'_0, x_0; E) = \frac{1}{i\hbar}\int dt\, e^{iEt/\hbar}\theta(t)\big\langle\{\psi_{Ln'\nu'}(x'_0,t), \psi^\dagger_{Rn\nu}(x_0,0)\}\big\rangle$ with $\psi_e = \psi$ and $\psi_h = \psi^\dagger$ in terms of the original field operators in Hamiltonian (1). Both x'_0 and x_0 are chosen far away from the QPC so that the scattering channels are well-defined; the explicit choice of x'_0 and x_0 is otherwise not important.

The scattering matrices are constrained by PHS and TRS, respectively, as (see Supplemental Material[62]

Sec. II.A):

$$S_{n'\nu',n\nu}(E,\varphi_{1,2}) = S_{n'\bar{\nu}',n\bar{\nu}}(-E,\varphi_{1,2})^*, \quad (15)$$

$$S_{n'\nu',n\nu}(E,\varphi_{1,2}) = -s_n s_{n'} S_{n\nu,n'\nu'}(E,-\varphi_{1,2}), \quad (16)$$

where $\bar{e} = h$, $\bar{h} = e$, and s_n is defined below Eq. (3). Eqs. (15) and (16) together imply that, at $E \simeq 0$ and $\varphi \simeq l\pi$, S takes the form

$$S_{0,\pi}(E \simeq 0) = \begin{pmatrix} 0 & b & -ia_1 & c \\ b & 0 & c^* & -ia_2 \\ ia_1 & c^* & 0 & b^* \\ c & ia_2 & b^* & 0 \end{pmatrix}, \quad (17)$$

in the same basis (1e, 2e, 1h, 2h) as in Eq. (12). Here, a_1 and a_2, both real, stand for local Andreev reflections involving either edge 1 or 2; b and c stand for normal back-scattering and crossed Andreev reflection, respectively, from one edge to the other. Note that normal back-scattering within one edge is forbidden by TRS (diagonal terms vanish). By further using the unitarity condition, S is limited down to two possibilities (see Supplemental Material[62] Sec. II.A):

$$\varphi \simeq 2l\pi : \quad c = 0, b \neq 0, a_1 = -a_2\,; \quad (18)$$

$$\varphi \simeq (2l+1)\pi : \quad b = 0, c \neq 0, a_1 = a_2\,. \quad (19)$$

The latter case reproduces Eq. (12) by identifying $a_1 = a_2 = iA/\Gamma$ and $c = -C/\Gamma$. Physically, the above equations imply that the zero-energy scattering processes at the QPC-SC interface will be entirely Andreev reflections, local and crossed, in the presence of MBSs at $\varphi \simeq (2l+1)\pi$; the crossed Andreev reflection probability will be gradually suppressed to zero when φ is tuned towards $2l\pi$, meanwhile normal scattering between edges will become finite. This is again consistent with our previous result Eq. (13) based on perturbation to the effective Hamiltonian (9).

The switching between normal backscattering and crossed Andreev reflection will be clearly manifested in zero-temperature multi-terminal differential conductances, defined by $G_{mn} = dI_m/dV_n$. In particular, we find at zero bias,

$$G_{21} = (|b|^2 - |c|^2)e^2/h, \quad (20)$$

which can be measured by biasing only contact 1 and grounding contacts 2 and 3. This expression is valid even in the absence of TRS, by interpreting in general b as $S_{2e,1e}$, and c as $S_{2h,1e}$. When φ is tuned across a multiple of π, G_{21} will oscillate with two sign flips in each 2π-period (see Fig. 4 upper panel) [65]. The switching of the backscattering current nature can also be seen explicitly in the zero-frequency current cross-correlation function between contacts 1 and 2 (while contact 3 is always grounded), defined by $P_{12} = \int_{-\infty}^{\infty} dt\, \frac{1}{2}\langle\{\delta\hat{I}_1(t), \delta\hat{I}_2(0)\}\rangle$ with current fluctuation $\delta\hat{I}_{n=1,2}(t) = \hat{I}_n(t) - \langle\hat{I}_n\rangle$. Within

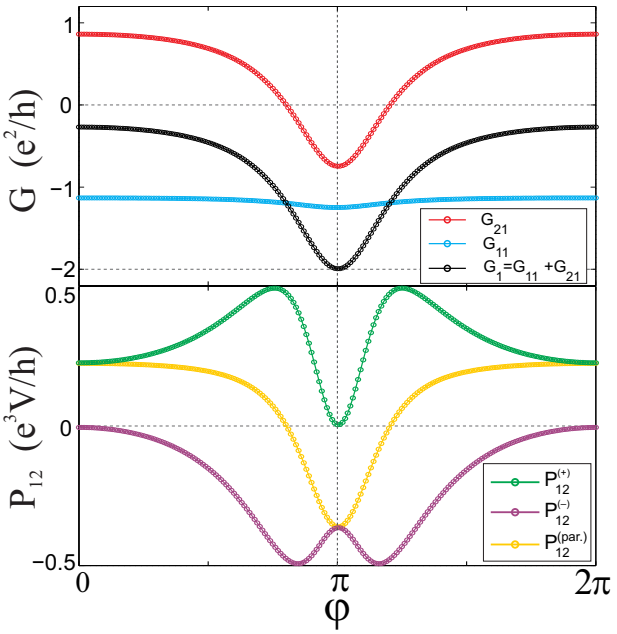

FIG. 4. Simulation results of two types of measurements on our proposed setup: differential conductances (upper panel) and zero-frequency current cross-correlators (lower panel), obtained numerically by using the Bogoliubov-de Gennes form of the Bernevig-Hughes-Zhang Hamiltonian [52]. These results verify and complement the features analyzed by using the effective edge theory (see main text).

the scattering approach [60, 66–69], the scattering matrix in Eq. (17) implies (see Supplemental Material[62] Sec. II.B):

$$P_{12}^{(+)} = 2\frac{e^3V}{h}a_1^2|b|^2, \quad P_{12}^{(-)} = -2\frac{e^3V}{h}a_1^2|c|^2, \quad (21)$$

where $P_{12}^{(+/-)}$ is the current cross-correlator measured with contacts 1 and 2 biased equally/oppositely. These formulas, valid for low bias voltage at $\varphi \simeq l\pi$, enable a straightforward examinations of the suppression of normal backscattering ($P_{12}^{(+)}$) or crossed Andreev reflection ($P_{12}^{(-)}$). More generally, we find that the following relation holds for all φ (see Supplemental Material[62] Sec. II.B and Fig. 4 lower panel):

$$P_{12}^{(+)} + P_{12}^{(-)} - P_{12}^{(\mathrm{par.})} = 0, \quad (22)$$

where $P_{12}^{(\mathrm{par.})} = -(e^3V/h)(G_{11}G_{21} + G_{12}G_{22})$ is conventionally called the partition noise [60]. The partition noise is composed of multiplications of G's, and hence also exhibits sign-flipping oscillations with varying magnetic flux (see Fig. 4 lower panel).

So far our analysis relied on one-dimensional effective edge theory and symmetry constraints. We further corroborate our conclusions by performing numerical simulations with the microscopic Bernevig-Hughes-Zhang

Hamiltonian [52] in two dimensions (see Supplemental Material[62] Sec. II.C). These simulations include explicitly the metallic contacts in our proposed setup shown in Fig. 1, and allow one to add various perturbations. Our main results, shown in Fig. 4, agree very well with the predictions of Eqs. (18-22). In addition, we verify that the switching from normal to Andreev scattering processes between two contacts (1 and 2) is a robust signature of the presence of the MBSs, which: i) remains valid when a finite ϵ_0 is taken into account; ii) persists even when the QSH sample region covered by the SC is slightly doped; iii) vanishes if the region covered by the SC does not support any helical edge states (i.e. topologically trivial).

Finally, we estimate the magnetic field and the temperature required to access the predicted transport signatures. From Ref. 70, the width of edge modes in InAs/GaSb quantum wells is estimated to be about 250 nm, therefore the device width in our proposal has to be larger than 500 nm. Combined with a device length about 1 μm, a magnetic field of 2 mT is needed to generate a half of the magnetic flux quantum. From Ref. 61, the energy gap of the proximity-effect induced superconductivity in InAs/GaSb quantum wells was observed to be around a few Kelvins, which is much larger than the base temperature (about 10 mK) that can be readily reached in a conventional dilution refrigerator. This intermediate range allows for reasonable QPC tunability for the coupling energy between the helical edge modes and the Majorana Kramers pairs, such that the proposed signature will not be suppressed by mere temperature effects. We emphasize that this signature, featuring tunable sign reversals of multi-terminal differential conductances, cannot be explained by other effects that can lead to zero bias peaks in simple nanowire setups (see the discussion of interaction effects in Ref. 71 and 72), and hence is a robust signature of Majorana Kramers pairs.

BAB and JL acknowledges support from ONR-N00014-14-1-0330 and MURI-130-6082. JL acknowledges support from Swiss National Science Foundation. BAB acknowledges support from NSF CAREER DMR-0952428, DARPA under SPAWAR Grant No. N66001-11-1-4110, the Packard Foundation, and the Keck grant. RL acknowledges the hospitality of the Aspen Center for Physics supported by NSF grant No. PHY-1066293, where part of this work was done. The work at Sandia was supported by the Department of Energy, Office of Basic Energy Sciences, Division of Materials Sciences and Engineering. Sandia National Laboratories is a multi-program laboratory managed and operated by Sandia Corporation, a wholly owned subsidiary of Lockheed Martin Corporation, for the U.S. Department of Energy's National Nuclear Security Administration under contract DE-AC04-94AL85000.

[1] F. Wilczek, Nat Phys **5**, 614 (2009).
[2] J. Alicea, Reports on Progress in Physics **75**, 076501 (2012).
[3] C. Beenakker, Annual Review of Condensed Matter Physics **4**, 113 (2013).
[4] T. D. Stanescu and S. Tewari, Journal of Physics: Condensed Matter **25**, 233201 (2013).
[5] S. R. Elliott and M. Franz, Reviews of Modern Physics **87**, 137 (2015).
[6] S. D. Sarma, M. Freedman, and C. Nayak, npj Quantum Information **1**, 15001 (2015).
[7] L. Fu and C. L. Kane, Physical Review Letters **100**, 096407 (2008).
[8] L. Fu and C. L. Kane, Physical Review B **79**, 161408 (2009).
[9] J. Nilsson, A. R. Akhmerov, and C. W. J. Beenakker, Physical Review Letters **101**, 120403 (2008).
[10] I. Knez, R.-R. Du, and G. Sullivan, Physical Review Letters **109**, 186603 (2012).
[11] W. Yu, Y. Jiang, C. Huan, X. Chen, Z. Jiang, S. D. Hawkins, J. F. Klem, and W. Pan, arXiv:1402.7282 [cond-mat] (2014).
[12] J. D. Sau, R. M. Lutchyn, S. Tewari, and S. Das Sarma, Phys. Rev. Lett. **104**, 040502 (2010).
[13] R. M. Lutchyn, J. D. Sau, and S. Das Sarma, Physical Review Letters **105**, 077001 (2010).
[14] Y. Oreg, G. Refael, and F. von Oppen, Physical Review Letters **105**, 177002 (2010).
[15] A. Cook and M. Franz, Physical Review B **84**, 201105 (2011).
[16] V. Mourik, K. Zuo, S. M. Frolov, S. R. Plissard, E. P. a. M. Bakkers, and L. P. Kouwenhoven, Science **336**, 1003 (2012), PMID: 22499805.
[17] L. P. Rokhinson, X. Y. Liu, and J. K. Furdyna, Nature Phys. **8**, 795 (2012).
[18] A. Das, Y. Ronen, Y. Most, Y. Oreg, M. Heiblum, and H. Shtrikman, Nature Physics **8**, 887 (2012).
[19] M. T. Deng, C. L. Yu, G. Y. Huang, M. Larsson, P. Caroff, and H. Q. Xu, Nano Lett. **12**, 6414 (2012).
[20] A. D. K. Finck, D. J. Van Harlingen, P. K. Mohseni, K. Jung, and X. Li, Phys. Rev. Lett. **110**, 126406 (2013).
[21] H. O. H. Churchill, V. Fatemi, K. Grove-Rasmussen, M. T. Deng, P. Caroff, H. Q. Xu, and C. M. Marcus, Phys. Rev. B **87**, 241401 (2013).
[22] M. T. Deng, C. L. Yu, G. Y. Huang, M. Larsson, P. Caroff, and H. Q. Xu, Scientific Reports **4**, 7261 (2014).
[23] P. Krogstrup, N. L. B. Ziino, W. Chang, S. M. Albrecht, M. H. Madsen, E. Johnson, J. Nygård, C. M. Marcus, and T. S. Jespersen, Nature Materials **14**, 400 (2015).
[24] T.-P. Choy, J. M. Edge, A. R. Akhmerov, and C. W. J. Beenakker, Physical Review B **84**, 195442 (2011).
[25] I. Martin and A. F. Morpurgo, Physical Review B **85**, 144505 (2012).
[26] S. Nadj-Perge, I. K. Drozdov, B. A. Bernevig, and A. Yazdani, Physical Review B **88**, 020407 (2013).
[27] J. Klinovaja, P. Stano, A. Yazdani, and D. Loss, Physical Review Letters **111**, 186805 (2013).
[28] B. Braunecker and P. Simon, Physical Review Letters **111**, 147202 (2013).
[29] M. M. Vazifeh and M. Franz, Physical Review Letters

111, 206802 (2013).
[30] F. Pientka, L. I. Glazman, and F. von Oppen, Physical Review B **88**, 155420 (2013).
[31] J. Li, T. Neupert, B. A. Bernevig, and A. Yazdani, Nature Communications **7**, 10395 (2016).
[32] S. Nadj-Perge, I. K. Drozdov, J. Li, H. Chen, S. Jeon, J. Seo, A. H. MacDonald, B. A. Bernevig, and A. Yazdani, Science **346**, 602 (2014).
[33] G. Moore and N. Read, Nuclear Physics B **360**, 362 (1991).
[34] C. Nayak and F. Wilczek, Nuclear Physics B **479**, 529 (1996).
[35] P. Bonderson, V. Gurarie, and C. Nayak, Physical Review B **83**, 075303 (2011).
[36] A. Y. Kitaev, Physics-Uspekhi **44**, 131 (2001).
[37] C. Nayak, S. H. Simon, A. Stern, M. Freedman, and S. Das Sarma, Rev. Mod. Phys. **80**, 1083 (2008).
[38] J. Alicea, Y. Oreg, G. Refael, F. von Oppen, and M. P. A. Fisher, Nature Phys. **7**, 412 (2011).
[39] K. T. Law, P. A. Lee, and T. K. Ng, Physical Review Letters **103**, 237001 (2009).
[40] K. Flensberg, Physical Review B **82**, 180516 (2010).
[41] L. Fidkowski, J. Alicea, N. H. Lindner, R. M. Lutchyn, and M. P. A. Fisher, Physical Review B **85**, 245121 (2012).
[42] A. R. Akhmerov, J. P. Dahlhaus, F. Hassler, M. Wimmer, and C. W. J. Beenakker, Physical Review Letters **106**, 057001 (2011).
[43] M. Wimmer, A. R. Akhmerov, J. P. Dahlhaus, and C. W. J. Beenakker, New Journal of Physics **13**, 053016 (2011).
[44] H.-J. Kwon, K. Sengupta, and V. M. Yakovenko, The European Physical Journal B - Condensed Matter and Complex Systems **37**, 349 (2004).
[45] M. Cheng and R. Lutchyn, Physical Review B **92**, 134516 (2015).
[46] J. Liu, A. C. Potter, K. T. Law, and P. A. Lee, Physical Review Letters **109**, 267002 (2012).
[47] D. Bagrets and A. Altland, Physical Review Letters **109**, 227005 (2012).
[48] D. I. Pikulin, J. P. Dahlhaus, M. Wimmer, H. Schomerus, and C. W. J. Beenakker, New Journal of Physics **14**, 125011 (2012).
[49] J. Männik and J. E. Lukens, Physical Review Letters **92**, 057004 (2004).
[50] J. Aumentado, M. W. Keller, J. M. Martinis, and M. H. Devoret, Physical Review Letters **92**, 066802 (2004).
[51] C. L. Kane and E. J. Mele, Phys. Rev. Lett **95**, 226801 (2005).
[52] B. A. Bernevig, T. A. Hughes, and S.-C. Zhang, Science **314**, 1757 (2006).
[53] M. Konig, S. Wiedmann, C. Brune, A. Roth, H. Buhmann, L. W. Molenkamp, X.-L. Qi, and S.-C. Zhang, Science **318**, 766 (2007).
[54] A. Roth, C. Brune, H. Buhmann, L. W. Molenkamp, J. Maciejko, X. Qi, and S. Zhang, Science **325**, 294 (2009).
[55] C. Liu, T. L. Hughes, X.-L. Qi, K. Wang, and S.-C. Zhang, Physical Review Letters **100**, 236601 (2008).
[56] I. Knez, R.-R. Du, and G. Sullivan, Physical Review Letters **107**, 136603 (2011).
[57] L. Du, I. Knez, G. Sullivan, and R.-R. Du, Physical Review Letters **114**, 096802 (2015).
[58] C. Schrade, A. A. Zyuzin, J. Klinovaja, and D. Loss, arXiv:1506.09120 [cond-mat] (2015).
[59] M. Büttiker, Physical Review Letters **57**, 1761 (1986).
[60] M. Büttiker, Physical Review B **46**, 12485 (1992).
[61] X. Shi, W. Yu, Z. Jiang, B. A. Bernevig, W. Pan, S. D. Hawkins, and J. F. Klem, Journal of Applied Physics **118**, 133905 (2015).
[62] See Supplemental Material [url], which includes Refs.73.
[63] In fact, the strict presence of TRS will imply the existence of another pair of MBSs at the opposite side of the Josephson junction. They are of no concern to us in terms of the local measurements that we propose.
[64] D. S. Fisher and P. A. Lee, Physical Review B **23**, 6851 (1981).
[65] Incidentally, the sum $G_1 = G_{11} + G_{21} + G_{31} = -2(|a_1|^2 + |c|^2)e^2/h$, reaches a quantized peak of magnitude $2e^2/h$ when φ is an odd multiple of π. Such quantization, however, is expect to require more stringent, currently unrealistic, experimental condition in order to observe than the sign reversals of G_{21}.
[66] M. P. Anantram and S. Datta, Physical Review B **53**, 16390 (1996).
[67] Y. M. Blanter and M. Büttiker, Physics Reports **336**, 1 (2000).
[68] J. Li, G. Fleury, and M. Büttiker, Physical Review B **85**, 125440 (2012).
[69] J. M. Edge, J. Li, P. Delplace, and M. Büttiker, Physical Review Letters **110**, 246601 (2013).
[70] V. S. Pribiag, A. J. A. Beukman, F. Qu, M. C. Cassidy, C. Charpentier, W. Wegscheider, and L. P. Kouwenhoven, Nature Nanotechnology **10**, 593 (2015).
[71] D. I. Pikulin, Y. Komijani, and I. Affleck, Physical Review B **93**, 205430 (2016).
[72] Y. Kim, D. E. Liu, E. Gaidamauskas, J. Paaske, K. Flensberg, and R. M. Lutchyn, arXiv:1605.02073.
[73] M. Konig, H. Buhmann, L. W. Molenkamp, T. Hughes, C.-X. Liu, X.-L. Qi, and S.-C. Zhang, J. Phys Soc. Jpn **77**, 031007 (2008).